

Detecting Many-Body Scars from Fisher Zeros

Yuchen Meng,¹ Songtai Lv,¹ Yang Liu,¹ Zefan Tan,¹ Erhai Zhao,^{2,*} and Haiyuan Zou^{1,†}

¹Key Laboratory of Polar Materials and Devices (MOE),

School of Physics and Electronic Science, East China Normal University, Shanghai 200241, China

²Department of Physics and Astronomy, George Mason University, Fairfax, Virginia 22030, USA

The far-from-equilibrium dynamics of interacting quantum systems still defy precise understanding. One example is the so-called quantum many-body scars (QMBSs), where a set of energy eigenstates evade thermalization to give rise to long-lived oscillations. Despite the success of viewing scars from the perspectives of symmetry, commutant algebra and quasiparticles, it remains a challenge to elucidate the mechanism underlying all QMBS and to distinguish them from other forms of ergodicity breaking. In this work, we introduce an alternative route to detect and diagnose QMBS based on Fisher zeros, i.e. the patterns of zeros of the analytically continued partition function Z on the complex β (inverse temperature) plane. For systems with scars, a continuous line of Fisher zeros will appear off the imaginary β axis and extend upward, separating the β plane into regions with distinctive thermalization behaviors. This conjecture is motivated from interpreting the complex Z as the survival amplitude of the thermofield double state, and it is validated by analyzing two models with QMBS, the $\bar{P}X\bar{P}$ model and the Ising chain in external fields. These models also illustrate another scenario of ergodicity breaking, where lines of Fisher zeros repeatedly intersect the imaginary β axis. This “statistical mechanics” approach places QMBS within the same framework of thermal and dynamical phase transitions. It has the advantage of easily spotting the emergence of scars without exhaustively examining each individual quantum state.

Introduction. The Eigenstate Thermalization Hypothesis (ETH) postulates that an isolated interacting quantum system typically thermalizes [1, 2]. But there are known cases of ETH being violated, even in non-integrable systems free of disorder. A prominent example is quantum many-body scars (QMBSs) [3–7] which have been observed in various platforms [8–11]. Roughly speaking, a set of energy eigenstates, usually equally spaced to form a tower structure, become decoupled from the rest of the spectrum and give rise to persistence oscillations. The mechanism by which QMBS evade ETH has been attributed to Krylov-restricted Hilbert space fragmentation, spectrum-generating algebras, commutant algebras, or projector embeddings [12–15], and they can also be understood from a quasiparticle perspective [16]. Key properties of QMBS are typically explored by the energy spectrum, entanglement entropy, Loschmidt echo, and other features of the Hamiltonian and its eigenstates. In contrast to QMBS, there are systems that strongly break ETH (SBETH) [17], leading to more profound deviations from thermal equilibrium. Examples include oscillations described by quasiparticles [18–20] and Continuous Time Crystals [21–26], which spontaneously break time-translation symmetry. Possible connection between QMBS and SBETH has been suggested [27]. A unifying theoretical framework for all known QMBS, however, is still lacking. Currently, to find new instances of scarred states in candidate Hamiltonians, one must hand-select a few states and monitor their dynamics. The exhaustive search can turn prohibitively expensive for large system sizes, evocative of finding a needle in a haystack. Thus it is desirable to develop a diagnostic device that can spot the existence of QMBS while avoiding the inspection of each individual state.

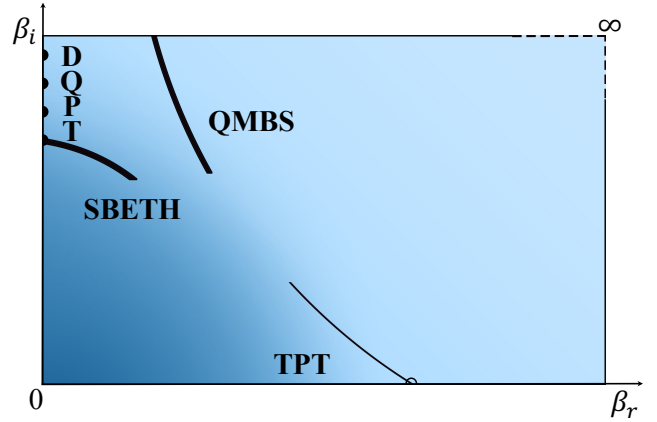


FIG. 1. The lines of Fisher zeros on the complex $\beta = \beta_r + i\beta_i$ plane in the thermodynamic limit, with darker regions indicating larger thermodynamic and smaller quantum fluctuations (schematic). The thin solid line represents the TPT in classical models. Empty circles on the β_r axis and solid circles on the β_i axis mark the TPT and DQPT points. The thick solid line touching the β_i axis corresponds to the SBETH model, while the one approaching but not touching it represents the QMBS model.

In this paper, we propose and demonstrate such an alternative approach based on Fisher zeros, a device invented originally to understand the singularities of equilibrium partition functions and thermal phase transitions (TPTs) [28–30]. The dynamical decoupling of scars from the bulk spectrum is reminiscent of phase separation and hints that the tools from statistical mechanics may help yield fresh insights. To formalize this idea, we follow Fisher and analytically continue the partition function

$Z = \sum_n e^{-\beta E_n}$ by allowing β to take on complex values, $\beta = \beta_r + i\beta_i$. Then Z becomes complex-valued, $Z = \sum_n e^{-\beta_r E_n} e^{-i\beta_i E_n}$, and describes the time evolution of a mixed ensemble at inverse temperature β_r and time $t = \beta_i$. The modulus square of Z , known as the spectral form factor, has been widely used in the study of quantum chaos [31]. To further connect Z to pure state dynamics, we can purify the mixed state by enlarging the Hilbert space, e.g., by making a copy R of the original system L and defining the thermofield double (TFD) state $|\Psi(\beta_r, 0)\rangle = \sum_n e^{-\beta_r E_n/2} |n\rangle_L \otimes |n\rangle_R$ [32]. Then Z is nothing but the returning amplitude of the pure TFD state evolving under the single Hamiltonian $H_L \otimes 1_R$, $Z(\beta_r, t) \sim \langle \Psi(\beta_r, 0) | \Psi(\beta_r, t) \rangle$, where the normalization factor is dropped for brevity and β_r serves as a parameter of Ψ that controls the weights of various eigenstates $|n\rangle$ [33]. If a system H_L contains scar states, they will continue to evade thermalization in the doubled system, for the added subsystem R acts merely as a bath. Thus, the existence of scars is bound to manifest in $Z(\beta_r, t)$ at long times if the initial TFD state $|\Psi(\beta_r, 0)\rangle$ contains sufficient amplitude $e^{-\beta_r E_n}$ of the scarred states. In other words, $Z(\beta_r, \beta_i)$ cannot be a smooth single-valued function free of qualitative changes when β_r is tuned continuously.

A conjecture about scars and Fisher zeros. These considerations lead to our main conjecture: *for a system with QMBS, at sufficiently large β_i , there exists a line of Fisher zeros on the complex β plane where Z vanishes.* As illustrated in Fig. 1, the line of zeros (labelled by QMBS) extends upward toward large β_i and marks the singularity of $\ln|Z|$ in the limit of large system sizes. When the line is crossed, e.g., by increasing β_r in the horizontal direction, the long-time dynamics of the TFD state will experience a qualitative change. Before we present numerical evidence to support this conjecture, it is illuminating to compare the location and implication of Fisher zeros in the present setting to their previous applications. In his seminar work on classical statistical models, Fisher observed that the zeros of $Z(\beta_r, \beta_i)$ pinching the β_r axis marks a TPT. In recent years, the concept of the complex-valued partition function and its zeros has been extended to the field of quantum many-body physics. For example, in quench dynamics following a given initial state ψ_i , one can define a boundary partition function $Z_i(\beta = it) = \langle \psi_i | e^{-\beta H} | \psi_i \rangle = \langle \psi_i | e^{-itH} | \psi_i \rangle$, which is analogous to Z except that β is restricted to the imaginary axis $\beta_i = t$. The zeros of Z_i on the β_i axis then mark dynamical quantum phase transitions (DQPTs) [34]. These known locations of Fisher zeros are shown by the empty and solid circles in Fig. 1 which identify TPT and DQPT respectively. In contrast, the zeros associated with QMBS are located away from either the real or the imaginary β axis. To our knowledge, the link between these Fisher zeros and breakdown of ETH has not been recognized before.

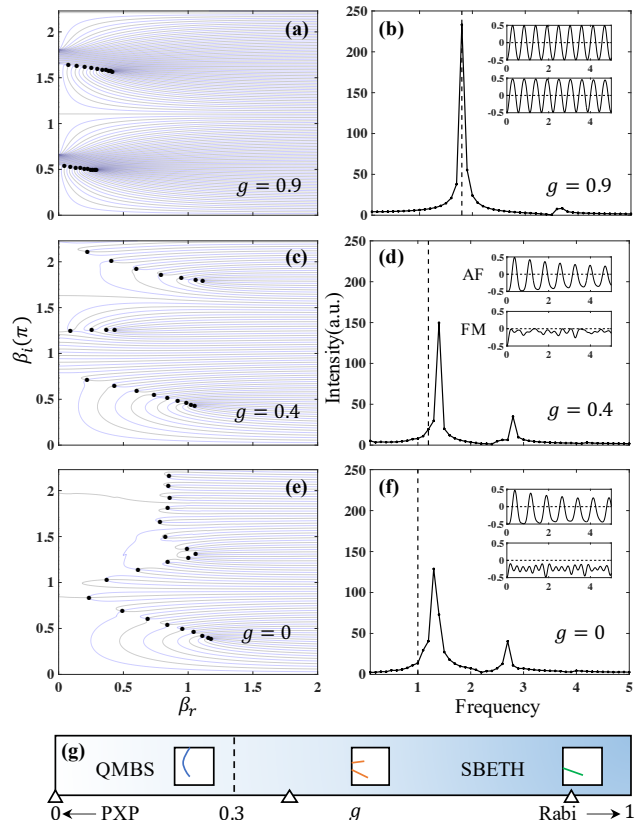


FIG. 2. Fisher zeroes and real-time dynamics in the $\bar{P}X\bar{P}$ model: (a), (c), and (e) depict the Fisher zeros of the system with $L = 32$ at $g = 0.9, 0.4$, and 0 , respectively. The blue and grey lines represent the zero solutions of real and imaginary part of Z , with their intersections marking the Fisher zeroes (black dots). Obtained from ED, (b), (d), and (f) show the frequency intensity of the AF state for the system with $L = 12$. The vertical dashed lines indicate the system's first energy gap. The upper and lower insets of each panel display the real-time oscillation curves of the AF and FM states (with time in units of 2π), respectively. (g) illustrates the two distinct regions of thermalization behavior based on g : QMBS ($0 \leq g \lesssim 0.3$) and SBETH ($0.3 \lesssim g < 1$).

One should bear in mind that the distribution of Fisher zeros on the complex β plane is model dependent and may appear more complicated than the simple schematics in Fig. 1. Previously, we have shown that the Fisher zeros provide valuable insight into the excitation spectrum and quantum critical dynamics [35–37]. This is not surprising because Z contains the interplay between quantum fluctuations (at large β) and thermal fluctuations (at small β) [37]. For example, the vanishing of Fisher zero lines at the infinity of the β plane identifies the quantum phase transition point in one-dimensional quantum spin models [35, 36]. Here, our primary focus is the distinctive feature of Fisher zeros near the β_i axis, for relatively large values of β_i , i.e., highly excited, long-

time dynamics.

There is yet another scenario of ergodicity breaking, labelled by SBETH in Fig. 1, in which the Fisher zeros repeatedly cross the β_i axis. Note that Fisher zeros are the zeros of Z , not to be confused with those of Z_i defined for a specific initial state in quench dynamics. In fact, $Z = \text{Tr} e^{-\beta H} = \sum_i Z_i$ where $\{|\psi_i\rangle\}$ form a complete basis. In other words, the presence of Fisher zeros on the β_i axis indicates a greater possibility for more $Z_i = 0$ solutions to cross the β_i axis. In this scenario, in contrast to the case of QMBS, the long-time region with small β_r value can be adiabatically connected to the large β_r regime on the β plane. However, going along the vertical direction near $\beta_r = 0$ will encounter non-analyticities of Z multiple times, indicating much stronger ETH breaking than QMBS (which is usually referred to as weak breaking of ETH). Our second conjecture is that the SBETH behaviors of Fisher zeros correspond to more complicated non-thermal behaviors at high temperature and long times. Note that QMBS and SBETH are not mutually exclusive, they can coexist.

We will first validate the above conjectures by constructing a new PXP -type model that incorporates a crossover from QMBS to SBETH. Then, using non-integrable models with Ising interactions, we further explore the rich interplays of the Fisher zeros associated with QMBS and SBETH when both are present. Taken together, these model studies reveal the distinct characteristics of each scenario and offer insights about the unifying link between Fisher zeros and ergodicity breaking. The observed commonalities point to potential application of the proposed approach to other systems. For example, we find that the Fisher zeros associated with QMBS approach but do not cross the imaginary β axis. In contrast, the Fisher zeros associated with SBETH systems repeatedly intersect the imaginary axis, inevitably giving rise to DQPTs.

The $\bar{P}X\bar{P}$ model. By extending from the Rydberg-blockade PXP model [3, 38, 39], we propose a $\bar{P}X\bar{P}$ model, whose Hamiltonian is

$$H = - \sum_{i=1}^L \bar{P}_i \sigma_{i+1}^x \bar{P}_{i+2}, \quad (1)$$

where σ_i^x is the Pauli x matrix operators on site i . The operator \bar{P} is designed as $\bar{P} = (|0\rangle\langle 0| + g|1\rangle\langle 1|)$ with $|0\rangle$ and $|1\rangle$ are two eigenstates of σ^z (Pauli z matrix). The tuning parameter $g \in [0, 1]$ allows for a connection between the PXP model ($g = 0$) and the non-interacting single spin flip model ($g = 1$).

We employ the tensor network method [40–42] to compute the complex Z and its Fisher zeros. Specifically, using Trotter decomposition, the partition function of a one-dimensional quantum system of length L can be mapped to a two-dimensional tensor network of size $L \times N$, where $N = \beta/\tau$ with the Trotter time τ [43].

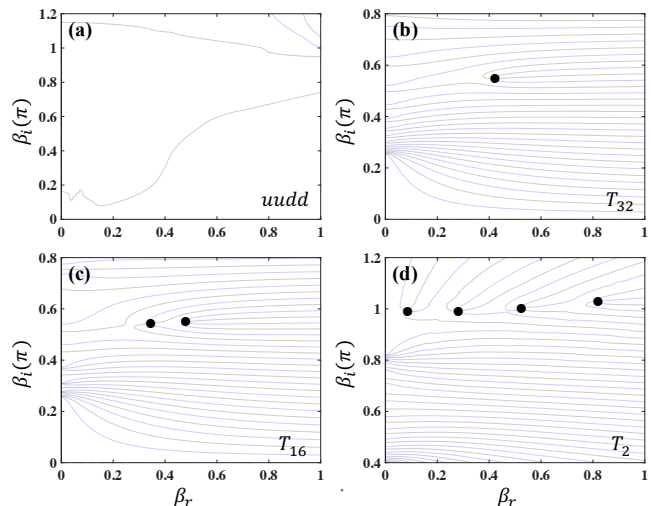


FIG. 3. The Fisher zeros of boundary partition function Z_i for different states in the $\bar{P}X\bar{P}$ model at $g = 0$ (the PXP model) with size $L = 32$: (a) $uudd$ state, (b) T_{32} state, (c) T_{16} state, and (d) T_2 state (or AF state). The markings of lines and points are the same as in Fig. 2. In (a), there are no zeros in the considered region, while (b)-(d) contain 1, 2, and 4 zeros, respectively. Their positions and the trend of approaching the β_i axis differ significantly.

We utilize the high order tensor renormalization group (HOTRG) algorithm [44] extended to complex β [45] to contract this two-dimensional network, determining the locations where the real and imaginary parts of Z vanish, thereby identifying the Fisher zeros through their intersections. In our calculations, we fix $N = 1024$, and $L = 32$ (noting that this method is capable of handling larger L , $L = 32$ is chosen here only for visualization purposes). The density of Fisher zeros increases with L . To capture the system’s non-thermal oscillatory behavior, we use exact diagonalization (ED) to perform long-time dynamical evolution $|\psi(\beta_i)\rangle = \exp(-i\beta_i H)|\psi_0\rangle$ [with the initial state ψ_0 chosen as the antiferromagnetic (AF) or ferromagnetic (FM) state] and measure the values of $\langle S_z \rangle = \langle \psi(\beta_i) | S_z | \psi(\beta_i) \rangle$ with $S_z = \sigma_z/2$ at any given site (with β_i up to 40π playing the role of time t) in the system $L = 12$. Given that the QMBS spectra and entanglement entropy of similar PXP -type models have already been extensively studied, we focus here on presenting the results of the two aforementioned “numerical experiments”, shown in Fig. 2. As Z is symmetric with respect to both the β_r and β_i axis, only the first quadrant is displayed.

At $g = 1$, the Fisher zeros are located at isolated points on the β_i axis, specifically at $\beta_i = \pi/2 + n\pi$. Correspondingly, all states, including AF and FM, undergo simple Rabi oscillations. As g decreases, the Fisher zeros extend from the β_i axis into the complex- β plane, forming small line segments. The lines of zeros of both the real

and imaginary parts of Z remain dense near the β_i axis [Fig. 2(a)]. Both AF and FM states still exhibit strong oscillatory behavior, with energy scales that correspond close to the system's low-energy excitations. In the small β_r region near the β_i axis, a vertical path will cut through these lines of zeros, suggesting that thermalization is hindered at long times. Since the small β_r region remains adiabatically connected to the large β_r region, the evasion of thermalization is closely related to the long lived low-energy excitations. Therefore, this parameter regime can be identified as being dominated by SBETH [Fig. 2(b)]. For $g \gtrsim 0.3$, as g further decreases, additional Fisher zero line segments begin to emerge between the previously formed small segments, while the density of zeros of both the real and imaginary parts of Z near the β_i axis gradually decreases [Fig. 2(c)]. Correspondingly, the system's dynamical behavior reveals oscillation frequencies far away from the low-energy excitations. The AF state maintains non-thermal oscillations, but with a gradually emerging secondary peak at roughly twice the frequency, corresponding to a tower-of-scars behavior. In contrast, the FM state no longer exhibits non-thermal oscillations but retains weak spin-flip effects. Therefore, this regime can be viewed as the crossover region between SBETH and QMBS [Fig. 2(d)]. Starting from $g \approx 0.3$, the Fisher zero lines begin to detach from the β_i axis and connect vertically [Fig. 2(e)]. Dynamically, only the AF state maintains non-thermal oscillations, marking the parameter regime $g \lesssim 0.3$ as dominated by QMBS [Fig. 2(f)]. This analysis highlights how varying g reveals distinct structures of Fisher zeros, providing a clear depiction of the crossover between QMBS and SBETH regimes [Fig. 2(g)].

QMBS and SBETH not only exhibit different configurations of the Fisher zeros of Z but also demonstrate distinct properties in the zeros of Z_i . At $g = 1$, the zeros of all the Z_i coincide with those of Z . As g decreases and the blockade interaction is introduced, the zeros of most Z_i remain close to the same position. This is also reflected in the dense lines of zeros for both the real and imaginary parts of Z in Fig. 2(a). In contrast, in the QMBS region, Z does not have zeros at $\beta_r = 0$ (the zero solutions no longer lie on the β_i axis), implying that the zeros of Z_i on the β_i axis (if they exist) cannot coincide at the same position. Consequently, the dynamical behavior of each state will be completely different. We verify this conclusion by calculating the zeros of Z_i for different states at $g = 0$ with $L = 32$. For a product state whose spin is configured with an up-up-down-down (*uudd*) pattern, we find that there are no zeros in a large region near the β_r and β_i axes [Fig. 3(a)]. We further consider different T_i states (defined as patterns like *uudd*..., where the number of down spins is $i - 1$). For states closer to the FM state, we find that there are only one and two zeros exists near the axes in the T_{32} and T_{16} state, respectively [Fig. 3(b)(c)], and their approach to the β_i axis

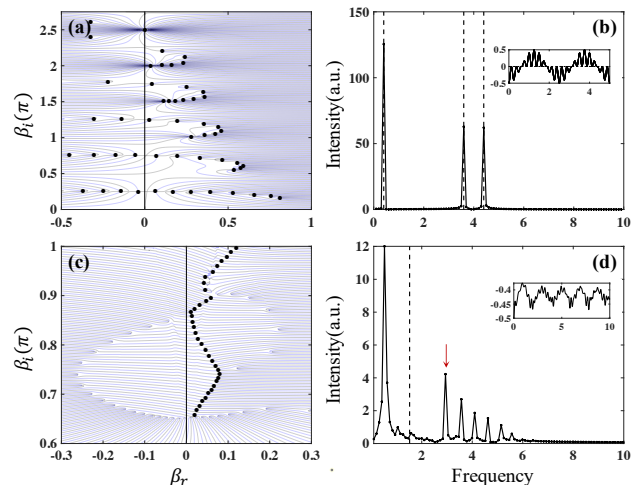


FIG. 4. Fisher zeros and real-time dynamics in the Ising model with external fields. The markings of lines and points are the same as in Fig. 2. (a) The Fisher zeros of the case $g_t = 0, h_l = 0.2$ in the system with $L = 32$, with the zeros are marked (black dots). (b) The dynamic spectrum of the $|\dots \rightarrow \dots\rangle$ state in the system with $L = 12$. Dashed lines correspond to the respective energy levels in the spectrum. (c) The Fisher zeros of the case $g_t = 0.5, h_l = 0.1$ in the system with $L = 128$, with only the zeros describing the scars marked. (d) The spectrum information of the FM state. Dashed lines correspond to the first excited state. The peak with red arrow is the scar peak, while others arising from finite-size effects exhibit a tower structure.

becomes slow as the system size increases. In contrast, for the scar state T_2 (or AF state), its zeros exhibit a clear tendency to approach the β_i axis, and the positions differ significantly from those of the T_{32} and T_{16} states [Fig. 3(d)]. Therefore, the differences in the zeros of Z_i for all possible states in the Hilbert space are responsible for the zeros of the total Z moving away from the imaginary axis.

Ising chain with external fields. To demonstrate the broad applicability of the Fisher zero behaviors observed for QMBS and SBETH, we examine another model with strong many-body interactions. Consider a one-dimensional Ising model with external fields, described by the Hamiltonian

$$H = - \sum_{j=1}^L (\sigma_j^z \sigma_{j+1}^z + g_t \sigma_j^x + h_l \sigma_j^z), \quad (2)$$

where g_t and h_l are the strength of the transverse and longitudinal fields, respectively.

We first consider the case where only the longitudinal field is present ($g_t = 0$). Z and Fisher zeros in this limit can be determined exactly. When $h_l = 0$, the Fisher zeros form lines parallel to the β_r axis, extending to $\beta_r = +\infty$. As h_l is introduced, these zeros terminate at finite values of β_r , yielding a structure similar to that observed near

$g = 1$ in the $\bar{P}X\bar{P}$ model. Taking $h_l = 0.2$ as an example, Figure 4(a) shows the zero configurations for this case. In the complex β plane, the positions of the zeros crossing the β_i axis exhibit periodicity. Additionally, the termination points of the zeros from different line sectors form an envelope curve with a larger period, indicating a proportional relationship between the two periodicities. We then select the product of eigenstates of σ_j^x ($|\cdots \rightarrow \cdots\rangle$ state) for dynamical evolution. Figure 4(b) illustrates the dynamical evolution of this state, revealing intricate SBETH oscillatory behavior, with frequencies matching those of certain excitations in the system's spectrum. The multiple oscillatory modes align with the periodicities of the Fisher zeros and the envelope curve described earlier.

We further consider the case where both h_l and g_t are present. The zeros in the absence of h_l can also be exactly solved [35]. For instance, at $g_t < 1$, the zero lines and closed loops alternately appear in the β plane. When h_l is introduced, the closed loops are broken up, enabling meson quasiparticle excitations that were previously confined within the loops to emerge [35]. Correspondingly, the Fisher zeros that were initially located on the β_i axis are displaced due to the effect of h_l , exhibiting characteristics associated with QMBS. The coexistence of these two types of Fisher zero configurations demonstrates that in strongly correlated models, quasiparticles can influence scar phenomena. Figure 4(c) provides an example of Fisher zeros for $g_t = 0.5$ and $h_l = 0.1$, showing a configuration similar to that in the $\bar{P}X\bar{P}$ model near $g = 0$. We use the FM state, which does not undergo DQPT, for the evolution. The oscillatory behavior and corresponding frequencies are shown in Fig. 4(d). We find that the peak at a frequency of 2.9 remains unchanged with system size and differs from the system's lowest-energy excitation. This peak corresponds exactly to the scar effect induced by meson excitations [6]. Although other nearly equally spaced peaks arise due to finite-size effects, they build upon the meson peak.

The significance of finding Fisher zeros. Given that the Lee-Yang zeros have already been experimentally detected by controlling external fields [46], it is reasonable to expect the experimental observation of Fisher zeros. While this is challenging because it requires coupling the complex β with the entire Hamiltonian, non-unitary evolution in quantum circuits [47, 48] offers a convenient way for potential realization and detection. In addition, the rapidly improving capacity to measure the many-body states of Rydberg atom system [8, 9] provide a possibility for probing the Fisher zeros in finite systems. For example, one can extract the effective temperature $1/\beta_r$ by fitting the decay of the Loschmidt ratio for different states. Summing over these states gives the total Z to reveal at which time it reaches zero. A detailed knowledge of Fisher zeros, e.g., from the tensor network calculation, also has theoretical significance. It can aid the

construction of parent Hamiltonians [49–51] to achieve novel quantum phases of matter which have been long hypothesized.

Conclusion. We demonstrate the distinct characteristics of QMBS and SBETH in the zeros of the complex partition function using the newly constructed $\bar{P}X\bar{P}$ model and a quantum many-body model that includes Ising interactions, confirming our conjecture about Fisher zeros and QMBS. The Fisher zeros characteristic of QMBS are close to the imaginary β axis but extend to large β_i , revealing a many-body renaissance in the dynamical region, which complements the many-body quasiparticle picture. On the other hand, SBETH arises alongside DQPTs and contains information from multiple specific energy levels of the system. Rydberg atoms provide a promising platform for experimentally probing Fisher zeros, offering a way to predict the Hamiltonian from novel phases of matter. Our work provides a new approach to understanding the unified formation mechanism of QMBS and studying the relationship between non-equilibrium dynamics and quantum fluctuations.

Acknowledgments. We thank Xiwen Guan, Gaoyong Sun, Junsen Wang, and Li You for helpful discussions. This work is supported by the National Natural Science Foundation of China (Grant No. 12274126). E.Z. acknowledges the support from NSF Grant PHY-206419, and AFOSR Grant FA9550-23-1-0598. We conducted part of this work during the 2nd Conference on “Quantum Simulations of Fundamental Physics” and the International Workshop on “Quantum Systems with Novel Spatiotemporal Control” in the fall of 2024 in Shanghai.

* ezhao2@gmu.edu

† hyzou@phy.ecnu.edu.cn

- [1] J. M. Deutsch, Quantum statistical mechanics in a closed system, *Phys. Rev. A* **43**, 2046 (1991).
- [2] M. Srednicki, Chaos and quantum thermalization, *Phys. Rev. E* **50**, 888 (1994).
- [3] C. J. Turner, A. A. Michailidis, D. A. Abanin, M. Serbyn, and Z. Papić, Weak ergodicity breaking from quantum many-body scars, *Nature Physics* **14**, 745–749 (2018).
- [4] S. Moudgalya, N. Regnault, and B. A. Bernevig, Entanglement of exact excited states of affleck-kennedy-lieb-tasaki models: Exact results, many-body scars, and violation of the strong eigenstate thermalization hypothesis, *Phys. Rev. B* **98**, 235156 (2018).
- [5] M. Schechter and T. Iadecola, Weak ergodicity breaking and quantum many-body scars in spin-1 xy magnets, *Phys. Rev. Lett.* **123**, 147201 (2019).
- [6] A. J. A. James, R. M. Konik, and N. J. Robinson, Non-thermal states arising from confinement in one and two dimensions, *Phys. Rev. Lett.* **122**, 130603 (2019).
- [7] P. Sala, T. Rakovszky, R. Verresen, M. Knap, and F. Pollmann, Ergodicity breaking arising from hilbert space fragmentation in dipole-conserving hamiltonians, *Phys. Rev. X* **10**, 011047 (2020).

- [8] H. Bernien, S. Schwartz, A. Keesling, H. Levine, A. Omran, H. Pichler, S. Choi, A. S. Zibrov, M. Endres, M. Greiner, V. Vuletić, and M. D. Lukin, Probing many-body dynamics on a 51-atom quantum simulator, *Nature* **551**, 579–584 (2017).
- [9] D. Bluvstein, A. Omran, H. Levine, A. Keesling, G. Semeghini, S. Ebadi, T. T. Wang, A. A. Michailidis, N. Maskara, W. W. Ho, S. Choi, M. Serbyn, M. Greiner, V. Vuletić, and M. D. Lukin, Controlling quantum many-body dynamics in driven rydberg atom arrays, *Science* **371**, 1355–1359 (2021).
- [10] P. Zhang, H. Dong, Y. Gao, L. Zhao, J. Hao, J.-Y. Desaulles, Q. Guo, J. Chen, J. Deng, B. Liu, W. Ren, Y. Yao, X. Zhang, S. Xu, K. Wang, F. Jin, X. Zhu, B. Zhang, H. Li, C. Song, Z. Wang, F. Liu, Z. Papić, L. Ying, H. Wang, and Y.-C. Lai, Many-body hilbert space scarring on a superconducting processor, *Nature Physics* **19**, 120–125 (2022).
- [11] G.-X. Su, H. Sun, A. Hudomal, J.-Y. Desaulles, Z.-Y. Zhou, B. Yang, J. C. Halimeh, Z.-S. Yuan, Z. Papić, and J.-W. Pan, Observation of many-body scarring in a bose-hubbard quantum simulator, *Phys. Rev. Res.* **5**, 023010 (2023).
- [12] M. Serbyn, D. A. Abanin, and Z. Papić, Quantum many-body scars and weak breaking of ergodicity, *Nature Physics* **17**, 675–685 (2021).
- [13] S. Moudgalya, B. A. Bernevig, and N. Regnault, Quantum many-body scars and hilbert space fragmentation: a review of exact results, *Reports on Progress in Physics* **85**, 086501 (2022).
- [14] S. Moudgalya and O. I. Motrunich, Exhaustive characterization of quantum many-body scars using commutant algebras, *Phys. Rev. X* **14**, 041069 (2024).
- [15] N. Shiraishi and T. Mori, Systematic construction of counterexamples to the eigenstate thermalization hypothesis, *Phys. Rev. Lett.* **119**, 030601 (2017).
- [16] A. Chandran, T. Iadecola, V. Khemani, and R. Moessner, Quantum many-body scars: A quasiparticle perspective, *Annual Review of Condensed Matter Physics* **14**, 443–469 (2023).
- [17] M. C. Bañuls, J. I. Cirac, and M. B. Hastings, Strong and weak thermalization of infinite nonintegrable quantum systems, *Phys. Rev. Lett.* **106**, 050405 (2011).
- [18] M. Kormos, M. Collura, G. Takács, and P. Calabrese, Real-time confinement following a quantum quench to a non-integrable model, *Nature Physics* **13**, 246–249 (2016).
- [19] C.-J. Lin and O. I. Motrunich, Quasiparticle explanation of the weak-thermalization regime under quench in a non-integrable quantum spin chain, *Phys. Rev. A* **95**, 023621 (2017).
- [20] M. Collura, M. Kormos, and G. Takács, Dynamical manifestation of the gibbs paradox after a quantum quench, *Phys. Rev. A* **98**, 053610 (2018).
- [21] F. Wilczek, Quantum time crystals, *Phys. Rev. Lett.* **109**, 160401 (2012).
- [22] D. V. Else, B. Bauer, and C. Nayak, Prethermal phases of matter protected by time-translation symmetry, *Phys. Rev. X* **7**, 011026 (2017).
- [23] P. Kongkhambut, J. Skulte, L. Mathey, J. G. Cosme, A. Hemmerich, and H. Kefler, Observation of a continuous time crystal, *Science* **377**, 670–673 (2022).
- [24] T. Liu, J.-Y. Ou, K. F. MacDonald, and N. I. Zheludev, Photonic metamaterial analogue of a continuous time crystal, *Nature Physics* **19**, 986–991 (2023).
- [25] A. Greilich, N. E. Kopteva, A. N. Kamenskii, P. S. Sokolov, V. L. Korenev, and M. Bayer, Robust continuous time crystal in an electron–nuclear spin system, *Nature Physics* **20**, 631–636 (2024).
- [26] X. Wu, Z. Wang, F. Yang, R. Gao, C. Liang, M. K. Tey, X. Li, T. Pohl, and L. You, Dissipative time crystal in a strongly interacting rydberg gas, *Nature Physics* **20**, 1389–1394 (2024).
- [27] K. Bull, A. Hallam, Z. Papić, and I. Martin, Tuning between continuous time crystals and many-body scars in long-range *xyz* spin chains, *Phys. Rev. Lett.* **129**, 140602 (2022).
- [28] C. N. Yang and T. D. Lee, Statistical theory of equations of state and phase transitions. i. theory of condensation, *Phys. Rev.* **87**, 404 (1952).
- [29] T. D. Lee and C. N. Yang, Statistical theory of equations of state and phase transitions. ii. lattice gas and ising model, *Phys. Rev.* **87**, 410 (1952).
- [30] M. Fisher and W. Brittin, Statistical physics, weak interactions, field theory, *Lectures in Theoretical Physics* (Boulder: University of Colorado Press) vol VIIC (1965).
- [31] J. Maldacena, S. H. Shenker, and D. Stanford, A bound on chaos, *Journal of High Energy Physics* **2016**, 10.1007/jhep08(2016)106 (2016).
- [32] Y. Takahashi and H. Umezawa, Thermo field dynamics, *International journal of modern Physics B* **10**, 1755 (1996).
- [33] A. del Campo, J. Molina-Vilaplana, and J. Sonner, Scrambling the spectral form factor: Unitarity constraints and exact results, *Phys. Rev. D* **95**, 126008 (2017).
- [34] M. Heyl, A. Polkovnikov, and S. Kehrein, Dynamical quantum phase transitions in the transverse-field ising model, *Phys. Rev. Lett.* **110**, 135704 (2013).
- [35] Y. Liu, S. Lv, Y. Yang, and H. Zou, Signatures of quantum criticality in the complex inverse temperature plane, *Chinese Physics Letters* **40**, 050502 (2023).
- [36] Y. Liu, S. Lv, Y. Meng, Z. Tan, E. Zhao, and H. Zou, Exact fisher zeros and thermofield dynamics across a quantum critical point, *Phys. Rev. Res.* **6**, 043139 (2024).
- [37] Y. Liu, E. Zhao, and H. Zou, From complexification to self-similarity: New aspects of quantum criticality, *Chinese Physics Letters* **41**, 100501 (2024).
- [38] I. Lesanovsky and H. Katsura, Interacting fibonacci anyons in a rydberg gas, *Phys. Rev. A* **86**, 041601 (2012).
- [39] C. J. Turner, A. A. Michailidis, D. A. Abanin, M. Serbyn, and Z. Papić, Quantum scarred eigenstates in a rydberg atom chain: Entanglement, breakdown of thermalization, and stability to perturbations, *Phys. Rev. B* **98**, 155134 (2018).
- [40] R. Orús, A practical introduction to tensor networks: Matrix product states and projected entangled pair states, *Annals of Physics* **349**, 117 (2014).
- [41] J. I. Cirac, D. Pérez-García, N. Schuch, and F. Verstraete, Matrix product states and projected entangled pair states: Concepts, symmetries, theorems, *Rev. Mod. Phys.* **93**, 045003 (2021).
- [42] Y. Meurice, R. Sakai, and J. Unmuth-Yockey, Tensor lattice field theory for renormalization and quantum computing, *Rev. Mod. Phys.* **94**, 025005 (2022).
- [43] M. Suzuki, Relationship between d-dimensional quantum spin systems and (d+1)-dimensional ising systems: Equivalence, critical exponents and systematic approx-

- imants of the partition function and spin correlations, *Progress of Theoretical Physics* **56**, 1454 (1976).
- [44] Z. Y. Xie, J. Chen, M. P. Qin, J. W. Zhu, L. P. Yang, and T. Xiang, Coarse-graining renormalization by higher-order singular value decomposition, *Phys. Rev. B* **86**, 045139 (2012).
- [45] A. Denblyker, Y. Liu, Y. Meurice, M. P. Qin, T. Xiang, Z. Y. Xie, J. F. Yu, and H. Zou, Controlling sign problems in spin models using tensor renormalization, *Phys. Rev. D* **89**, 016008 (2014).
- [46] X. Peng, H. Zhou, B.-B. Wei, J. Cui, J. Du, and R.-B. Liu, Experimental observation of lee-yang zeros, *Phys. Rev. Lett.* **114**, 010601 (2015).
- [47] M. P. Fisher, V. Khemani, A. Nahum, and S. Vijay, Random quantum circuits, *Annual Review of Condensed Matter Physics* **14**, 335 (2023).
- [48] E. Granet, C. Zhang, and H. Dreyer, Volume-law to area-law entanglement transition in a nonunitary periodic gaussian circuit, *Phys. Rev. Lett.* **130**, 230401 (2023).
- [49] I. Affleck, T. Kennedy, E. H. Lieb, and H. Tasaki, Rigorous results on valence-bond ground states in antiferromagnets, *Phys. Rev. Lett.* **59**, 799 (1987).
- [50] R. Shen, Y. Guo, and S. Yang, Construction of non-hermitian parent hamiltonian from matrix product states, *Phys. Rev. Lett.* **130**, 220401 (2023).
- [51] Peter Zoller, Closing remarks at the 2nd Conference on ‘Quantum Simulations of Fundamental Physics’ (<https://m.koushare.com/live/details/37543>) and the International Workshop on ‘Quantum Systems with Novel Spatiotemporal Control’ (<https://m.koushare.com/live/details/38269>).